Refractive index sensor using Fibonacci sequence of gyroidal graphene and porous silicon based on Tamm plasmon polariton

Zaky A. Zaky[1] · **M. Al-Dossari[2]** · **Ensjam I. Zohny[1]** · **Arafa H. Aly[1]**

Abstract
In this paper, binary photonic crystal with a quasi-periodic sequence is investigated. A Fibonacci sequence of gyroidal graphene and porous silicon terminated by the gyroidal layer is proposed as a refractive index sensor. The refractive index or concentration of an analyte can be predicted based on the resonant dip of Tamm plasmon. The excellent optical properties of porous silicon and gyroidal graphene will contribute to enhancing the performance of the proposed sensor. The impact of various geometric parameters is investigated. Compared with the similar structure of periodic photonic crystals, the sensitivity and figure of merit enhanced from 188.8 to 1347.7 THz/RIU (higher 614%) and from 355,384 to 554,405/RIU (higher 56%), respectively. The high-performance results imply that the suggested Fibonacci sensor is suitable for gas detection and bio-sensing applications.

Keywords Photonic crystal · Fibonacci sequence · Quasi crystals · Gyroidal graphene · Tamm resonance · Porous silicon

1 Introduction

One-dimensional photonic crystal (1D-PC) is alternating layers that can prohibit the propagation of electromagnetic waves through it (Yablonovitch 2001; Zaky et al. 2021a, 2022a, b; Yablonovitch and Gmitter 1989; Aly et al. 2020, 2021a, b; Abd El-Ghany et al. 2020; Aly and Zaky 2019; Ye et al. 2019; Meradi et al. 2022; Tammam et al. 2021). Tamm resonance or as some call it, Tamm plasmon polariton, (TPP) is the trapping of electromagnetic waves at the interface between 1D-PhC and a metallic layer. TPP position can be adjusted by controlling the optical parameters of the structure such as permittivity or the thickness of layers. By filling one layer of the structure with an analyte of gas or liquid, the TPP dip will be affected any change in the concentration of this analyte. With knowing the position

✉ Zaky A. Zaky
zaky.a.zaky@science.bsu.edu.eg

[1] TH-PPM Group, Physics Department, Faculty of Science, Beni-Suef University, Beni-Suef 62521, Egypt

[2] Department of Physics, Faculty of Science, King Khalid University, Abha 62529, Saudi Arabia

of the TPP dip, the refractive index or concentration of the analyte can be predicted (Zaky and Aly 2020). TPP has been used in biosensors, switches, and filters (Auguié et al. 2014; Zaky and Aly 2021a; Zaky et al. 2021b, 2022c, d).

Binary photonic crystal with quasi-periodic sequence (QP-PhC) is a middle link between periodic and random configurations. QP-PhC can be designed in different sequences such as Thue–Morse, Fibonacci sequence (FS), Rudin Shapiro, Cantor, and period-doubling (Steurer and Sutter-Widmer 2007). QP-PhC is distinct from periodic PhC in that QP-PhC has amazing optical properties like the appearance of multiple photonic band gaps (PBG) (Pandey 2017). The word count rule is used to define FS, $S_n = S_{n-1} S_{n-2}$ for $n \geq 2$ with $S_0 = B$ and $S_1 = A$ (Shukla and Das 2018). So, the first few strings of the FS are S_0: B, S_1: A, S_2: AB, S_3: ABA, S_4: ABAAB, and S_5: ABAABABA. QP-PhC was fabricated from SiO_2 and TiO_2 using electron evaporation by Gellerman et al. (1994). They found a good similarity between the theoretical simulations and experimental results.

Two-dimensional materials like porous silicon (PSi) and gyroidal materials are very interesting optical materials that have been the subject of extensive research (Zaky et al. 2021c; Zaky and Aly 2021b; Prayakarao et al. 2015). Porous silicon is a very interesting prospect for photonic devices because of the wide index of refraction variation due to the ratio of pores control, as well as the comparatively simple manufacturing methods and low cost (Tammam et al. 2021; Wang et al. 2007; Zaky et al. 2020). Electrochemical etching can be used to build PSi multilayers (Wang et al. 2007). Besides PSi, the Mechanical, optical, electrical, and thermal properties of graphene are all outstanding. Because of the atomic thickness of graphene and the weakness of bending rigidity, monolayers of graphene have restrictions in different applications (Jung et al. 2017). To overcome these restrictions, the gyroidal shape of graphene has recently been developed. Gyroidal graphene (GG) structure is a three-dimensional geometry on a triply periodic minimum shape (Jung et al. 2017). GG is considered a porous material having pores of small or large size (Cebo et al. 2017; Nakanishi et al. 2020; Ma et al. 2019). Chemical vapor deposition (Cebo et al. 2017), inorganic templates from the butterfly nanostructure or self-assembly (Turner et al. 2013), selective laser melting (Ma et al. 2019), self-assembly of a triblock copolymer (Nakanishi et al. 2020), light-based 3D printing process (Hensleigh et al. 2018), solvent-free method (Feng et al. 2019), or controlled phase separation (Liu et al. 2015) have all been used in experiments to realize gyroidal structures.

Zaky et al. (2021d) proposed a refractive index sensor based on the excitation of Tamm resonance at the interface between sample/Ta_2O_5 multilayers and a gyroidal layer of metals. This design recorded a sensitivity of 6.7 THz/RIU, a figure of merit (FoM) of 6×10^3/RIU, and a quality factor (Q-factor) of 3×10^3. Then, they studied the impact of using the GG layer to excite Tamm resonance at the end of PSi multilayers (Zaky et al. 2021e). This design recorded an improvement in sensitivity of 18.6 THz/RIU, FoM 1.3×10^5/RIU, and Q-factor of 2.6×10^4. After that, they studied the effect of using a multilayer of GG and PSi terminated by GG to excite Tamm resonance (Zaky and Aly 2021b). Comparing a similar structure of PSi multilayer and graphene, this structure achieved FoM and sensitivity higher than 748% and 39.75%, respectively. Other THz studies and applications can be found in references (Huang et al. 2022; Lu et al. 2022; Sheng et al. 2022; Lv et al. 2022; Li et al. 2022; Luo et al. 2021).

In this paper, we aim to enhance the performance of the sensor by proposing a novel GG/PSi FS-PhC sensor terminated by the GG layer is proposed. The impact of various optical parameters is investigated. Table 1 demonstrates that the suggested design outperformed all other structures. The use of completely porous materials is largely responsible for the high sample volume fraction relative to the volume fraction of the structure that increases the

Table 1 A comparison study

Reference	S (THz/RIU)	FoM (/RIU)	Materials
Keshavarz and Alighanbari (2019)	0.7	10.3	Tamm with graphene
Rezagholizadeh et al. (2020)	1.6	24.5	Graphene disks
He et al. (2020)	1.7	7	Graphene metamaterials
Zaky and Aly (2021c)	4.75	475	Graphene and PSi
Zaky et al. (2021e)	18.6	126,835	GG and PSi-PC
Zaky and Aly (2021b)	188.8	355,384	GG and PSi/graphene gyroid-PC
This work	1347.7	554,405	FS of GG and PSi

performance. Besides, we replaced the metallic layer with a GG layer to excite the Tamm state to overcome the easier corrosion of the thin metallic layer.

2 Basic equations and materials

In the Schematic diagram illustrated. FS (S_4) of GG and PSi terminated by the GG layer is proposed. N represents many times the S_4 FS will be repeated (N=4). A sample layer separates between the FS and GG layers to enhance the performance of the design (Zaky et al. 2021e; Zaky and Aly 2021c), as clear in Fig. 1. The sample enters the sensor package from the sample flow inlet to fill the pores of PSi and the cavities inside the GG layers.

The GG's optical constant can be determined as a function of the thickness of the gyroidal layer (d_{gyr}), effective plasmon frequency (λ_g), helix radius (r_g), the unit cell size of gyroid (a), volume fraction (f), and wire turn length (l_g) follows (Zaky et al. 2021e; Farah et al. 2014; Bikbaev et al. 2017):

$$\varepsilon_{gyr}(\omega) = \frac{l_g \sqrt{2}}{a}\left[1 - \left(\frac{4r_g}{\lambda_g}\right)^2 \left(\frac{\pi\sqrt{-\varepsilon_G(\omega)}}{2\sqrt{2}n_s} - 1\right)^2\right], \tag{1}$$
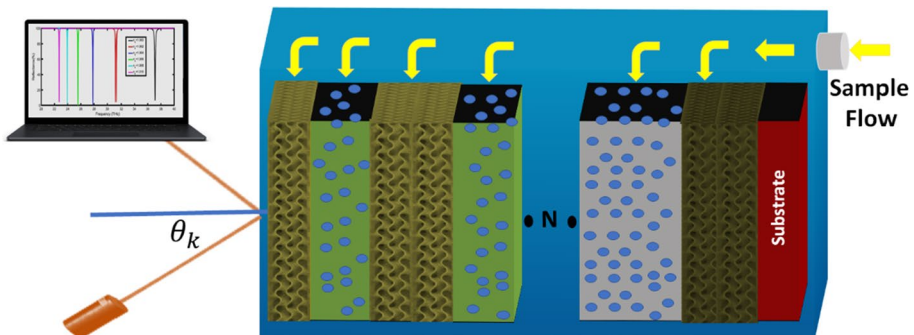

Fig. 1 Schematic diagram of the FS of GG/porous Si

$$l_g = \sqrt{(2\pi R)^2 + a^2} = a\sqrt{\frac{\pi^2\left(\sqrt{2}-1\right)^2}{4} + 1}, \tag{2}$$

$$R = \frac{\left(\sqrt{2}-1\right)^2}{4} + 1, \tag{3}$$

$$r_g = a\sqrt{f}\frac{\sqrt[4]{2}}{\sqrt{\pi\left[\sqrt{2+\pi^2} + \sqrt{2+\left(3+2\sqrt{2}\right)\pi^2}\right]}}, \tag{4}$$

$$\lambda_g = 1.15\,a\sqrt{1 - 0.65 lnf}. \tag{5}$$

For more details about the gyroidal model, see references Bikbaev et al. (2017), Abueidda et al. (2019). Using the approximate local random phase, the conductivity (σ) of one or a few sheets of graphene in the THz range of electromagnetic waves can be estimated from the intra-conductivity as a function of the number of graphene layers (G), Fermi energy (E_F), relaxation time (τ), and angular frequency (ω) (Zaky and Aly 2021b, 2021c; Bludov et al. 2013):

$$\sigma = G\frac{ie^2 E_F}{\pi\hbar^2\left(\omega + \frac{i}{\tau}\right)}. \tag{6}$$

The dispersion curve of porous silicon's refractive index (n_{Psi}) as a function of the refractive index of analyte filling the pores (n_s), the ratio of analyte (P), and silicon refractive index ($n_{Si} = 3.42$) is defined by Bruggeman's effective medium equation (Salem et al. 2006):

$$n_{Psi} = 0.5\sqrt{\psi + \sqrt{\psi^2 + 8n_{si}^2 n_s^2}},$$
$$\psi = 3P\left(n_s^2 - n_{si}^2\right) + \left(2n_{si}^2 - n_s^2\right). \tag{7}$$

The reflectance (R) of the TM polarized light will be simulated using the transfer matrix method (TMM) to study the response of the proposed design to the incident light (Yeh 1988; Zaky et al. 2021f; Born and Wolf 2013). The optical response of the proposed structure (R) can be calculated as:

$$R(\%) = 100 \times \lfloor r \rfloor^2, \tag{8}$$

where

$$r = \frac{\left(A_{11} + A_{12}p_s\right)p_0 - \left(A_{21} + A_{22}p_s\right)}{\left(A_{11} + A_{12}p_s\right)p_0 + \left(A_{21} + A_{22}p_s\right)}, \tag{9}$$

$$\begin{vmatrix} A_{11} & A_{12} \\ A_{21} & A_{22} \end{vmatrix} = \left(a_A a_B a_A a_A a_B\right)^N / a_s / a_{gyr}, \tag{10}$$

$$p_k = \frac{cos\left(\theta_k\right)}{n_k}, \tag{11}$$

where θ_k, n_k, a_k, p_0, and p_s are the incident angle, the refractive index of each layer, the transfer matrix element of each layer, related to the medium where the wave will be incident from, and the value of p for the substrate. TM polarization is when the incident electromagnetic waves' electric field vector is parallel to the incidence plane. TMM makes it simple to compute transmittance, reflectance, or absorbance spectra in both incoherent and coherent conditions (Katsidis and Siapkas 2002). TMM was used for simulating switches (Ahmed et al. 2017), solar cells (Aly and Sayed 2017), smart windows (Zaky and Aly 2022), and sensors (Zaky et al. 2022e, 2022f).

2.1 Results and discussions

As clear in the schematic diagram, it is proposed that the electromagnetic waves travel through the air and hits the first GG layer at an incident angle θ_0. A GG layer is placed on the end of the FS to excite Tamm resonance. The thickness of layers are $d_A = 100$ nm, $d_B = 200$ nm, $d_s = 4000$ nm and $d_{gyr} = 200$ nm. For layer A, a = 10 nm and f = 2%. But for the terminal layer of GG, a = 20 nm, and f = 20%. E_f and τ are taken with 1 eV and 1 ps, respectively. The porosity of the PSi layer is 50%. The angle of incidence is chosen to be $\theta = 0°$ as an initial condition, then it will be changed in the following studies to be optimized.

Figure 2a clears the reflectance spectra without and with the GG layer. Without a cap gyroidal layer, a wide PBG extended from 0.2 to 40 THz. The appearance of PBG is the result of the periodicity of two layers (GG and PSi) with high refractive index contrast. The resonant Tamm dip occurs only in the case of using the cap gyroidal layer at 31.6198 THz at $n_s = 1.000$. The underlying physics of the proposed design is that the resonant dip is very sensitive to any change in the effective refractive index of the structure. By changing the concentration of the gas sample than will be detected, the effective refractive index will change, and the position of the resonant dip with change. So, from the position of the resonant dip, we can predict the concentration of the sample.

As clear in Fig. 2b, for using samples with refractive indices of 1.002, 1.004, 1.006, 1.008, and 1.010 the resonant Tamm dips are located at 31.5504, 31.4814, 31.4125, 31.3440, and 31.2757, respectively.

Sensitivity (S), the figure of merit (FoM), the limit of detection (LoD) and quality factor (Q) will be calculated as a function of the increase in the refractive index of the sample (Δn_S), the shift in resonant frequency (Δf_R) and bandwidth (*FWHM*) for the structure to be evaluated compared to other studies (Ayyanar et al. 2018; Panda and Devi 2020):

$$S = \frac{\Delta f_R}{\Delta n_s}, \tag{12}$$
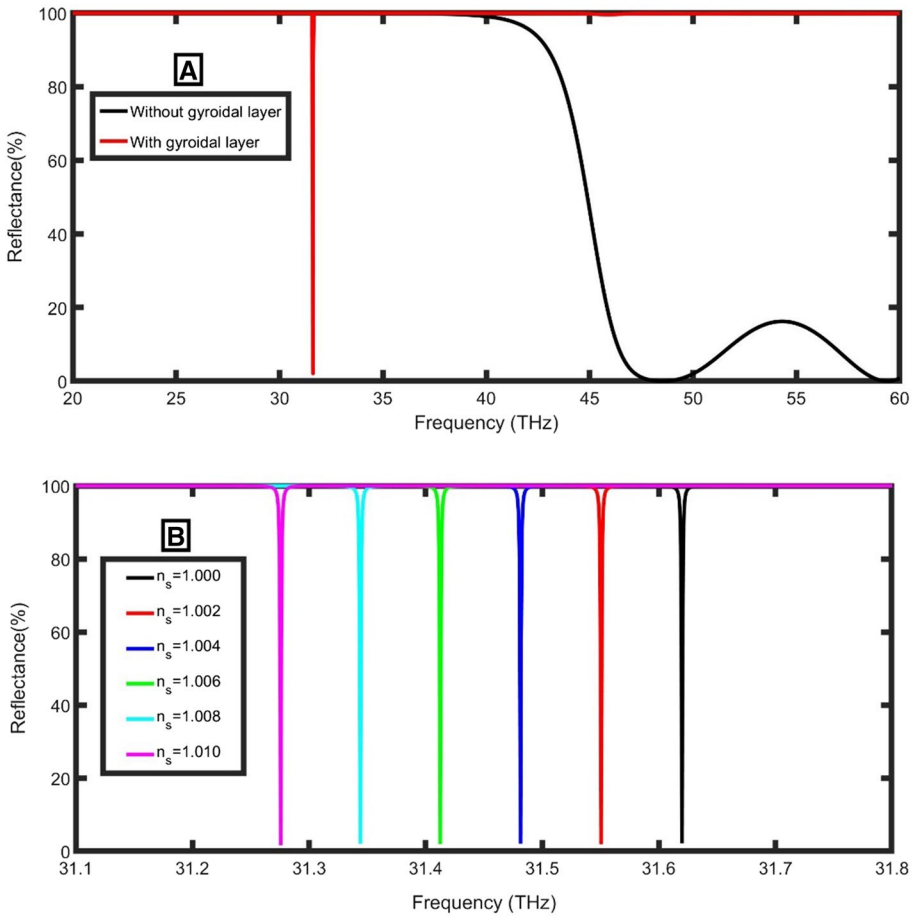
$$FoM = \frac{S}{FWHM}, \tag{13}$$

Fig. 2 The reflectance spectra of the terahertz biosensor **a** with and without GG at $n_{sample} = 1$, **b** at different n_{sample}

$$Q = \frac{f_R}{\text{FWHM}} . \tag{14}$$

According to the calculations, the sensitivity, FoM and Q of the proposed Fibonacci sensor is 34.41 THz/RIU, 35,269 RIU^{-1}, and 32,057.

Strong changes in the sensitivity, FWHM, FoM and Q-factor are observed when the incident angle was changed from 0° to 89° (Fig. 3). As the incident angle was changed from 0° to 80°, the sensitivity increased to record the highest value of 87.06 THz/RIU, then it slightly decreased (Fig. 3a). From Fig. 3b, the increase of the angle from 0° to 80° shows a clear increase in the FWHM that negatively affects the resolution of the structure. For angles higher than 80°, FWHM strongly decreases that positively affecting the resolution of the structure. Besides, the FoM and Q-factor strongly decrease from 0° to 80°, then slightly increase (Fig. 3b). To ensure that this sensor records high sensitivity with low FWHM, the angle of 89° will be used in the following calculations. To explain this increase in sensitivity with the incident angle, let a ray of light penetrates a sample layer with a thickness of 3 nm as clear in Fig. 3c. The optical path through the layer increases
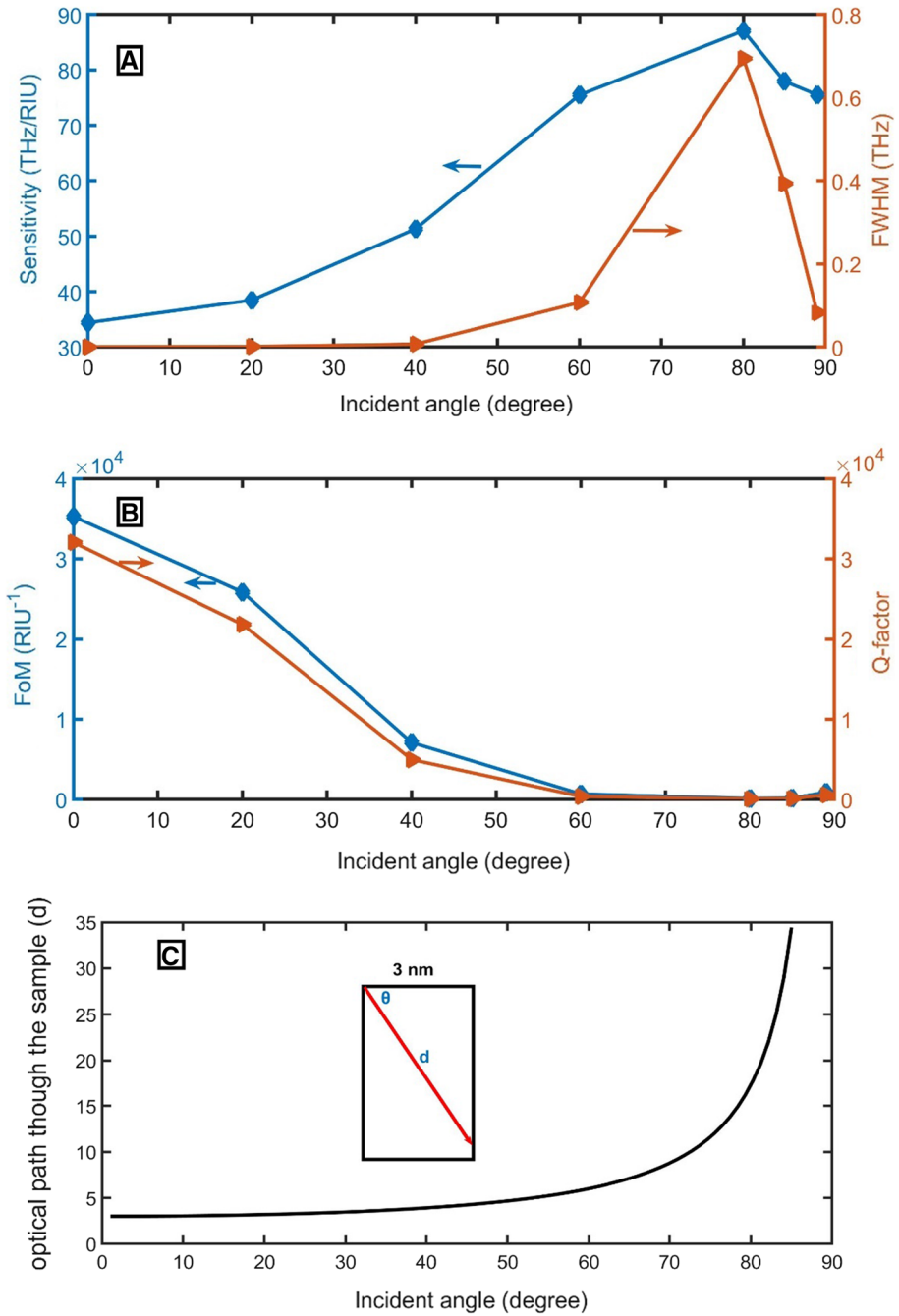
Fig. 3 The impact of changing the incident angle on the proposed Fibonacci sensor **a** sensitivity and FWHM, **b** FoM and Q-factor, and **c** the relation between the incident angle and the optical path inside a sample layer with thickness d

slightly at low angles and strongly increases at high angles. Due to the increase of the optical path through the sample layer, the sensitivity increases.

To enhance the performance of the sensor, the impact of changing the sample layer thickness will be studied in Fig. 4. As the sample layer thickness changes from 4000 to 20,000 nm, the sensitivity strongly increases due to the increase of light path through the sample and the increase of the interaction and light confinement. Then, as a result of saturation, it doesn't change for more increase in thickness (Fig. 4a). Besides, as we increase the sample layer thickness from 4000 to 7000 nm, FWHM strongly increases from 0.001 to 0.081 THz. For changing the thickness from 7000 to 15,000 nm, FWHM slightly decreases to 0.068 THz. For more increases in the thickness, FWHM does not change.

It is clear in Fig. 4b that with increasing the sample thickness from 4000 to 7000 nm, FoM strongly decreases from 77,416 to 2119 RIU^{-1}. For changing the thickness from 7000 to 15,000 nm, FoM slightly increases to 18,790 RIU^{-1}. For more increases in the thickness, FoM does not change. Also, the Q-factor decreases first and then does not change. The thickness of 25,000 nm will be selected as the sample layer thickness in the following studies.
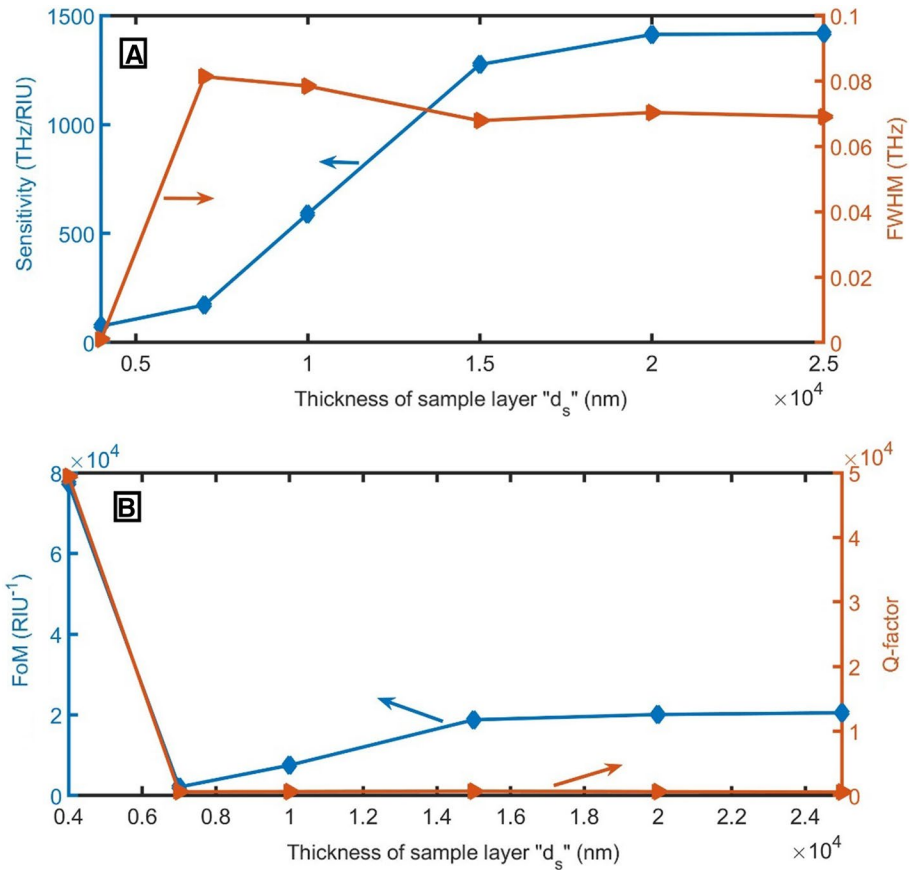

Fig. 4 The impact of changing the sample layer thickness on the proposed Fibonacci sensor **a** sensitivity and FWHM and **b** FoM and Q-factor

Figure 5 studies the impact of the thickness of layer A on the sensor performance. As clear in Fig. 5a, the sensitivity and FWHM slightly decrease as d_A increases. On the other hand, the FoM and Q-factor strongly increase as d_A increases from 10 to 100 nm, then slightly increases. The thickness of 30 nm will be the optimum because it records moderate performance as clear in Fig. 5b. Besides, the thickness of 30 nm achieves the lowest reflectance (highest confinement of electromagnetic waves).

Figure 6 clear the reflectance spectra generated under an incident angle of 89° of TM polarized electromagnetic waves. At the optimum conditions, by adjusting the sample refractive index from 1.000 to 1.002, 1.004, 1.006, 1.008 and 1.010, the resonant dip was moved to lower frequencies from 37.1088 THz, 31.2475 THz, 27.8125 THz, 25.86 THz, 23.9428 THz and 22.7082 THz.

In Table 1, the suggested Fibonacci sensor is compared with recently suggested sensors. The recommended Fibonacci sensor has distinguished sensitivity and FoM. The high-performance results imply that the suggested Fibonacci sensor is suitable for gas detection and bio-sensing applications.
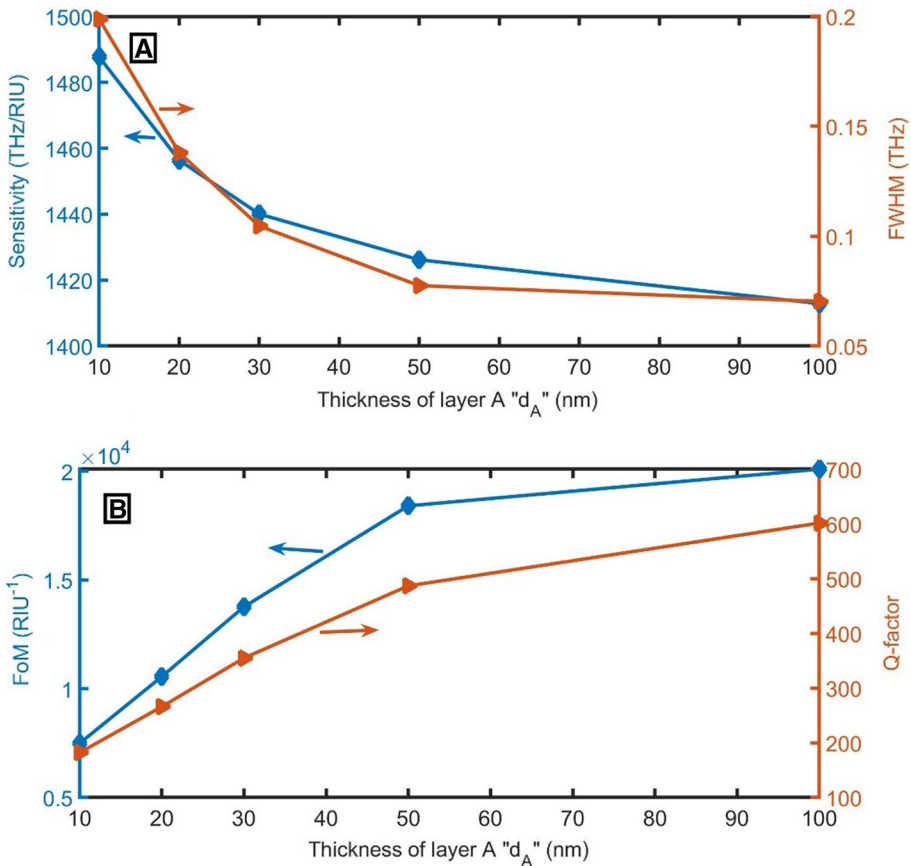

Fig. 5 The impact of changing the thickness of layer A (d_A) on the proposed Fibonacci sensor **a** sensitivity and FWHM and **b** FoM and Q-factor
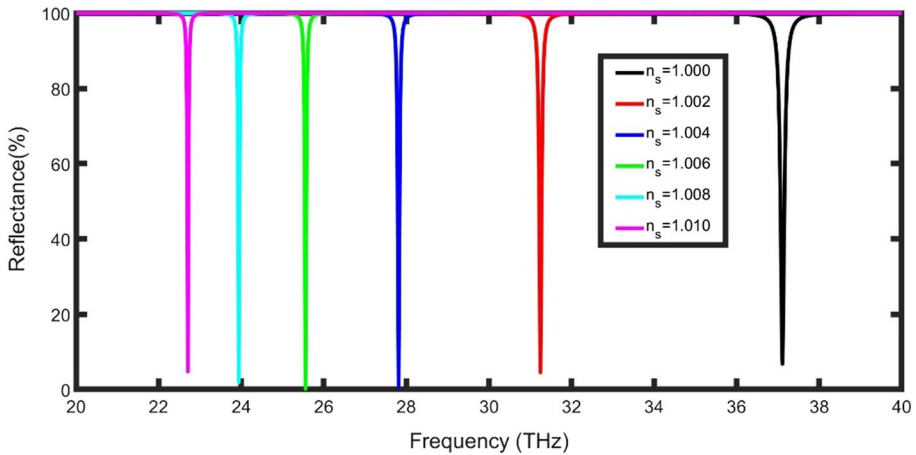
Fig. 6 The impact of changing the refractive index of the sample on the proposed Fibonacci sensor at optimum conditions

3 Conclusion

We proposed a novel GG/PSi FS-PhC sensor terminated by the GG layer for the detection of the refractive index. By changing the effective refractive index of the FS-PhC, the position of Tamm dips changes. The recommended Fibonacci sensor has distinguished sensitivity and FoM. Comparing the suggested FS-PhC structure to other similar sensors of periodic PhC, it was observed that the suggested structure has a superior FoM and sensitivity, even though it has a simple design that will not require polarizing matching components such as gratings or prisms. Because the thin metal film is readily eroded by corrosion, graphene is recommended to activate TPP.

Author contributions ZAZ corresponding author invented the original idea of the study, implemented the computer code, performed the numerical simulations, analyzed the data, wrote and revised the main manuscript text. MA-D discussed the results and supervised this work. EIZ discussed the results and supervised this work. AHA reviewed, edited, discussed the results, and supervised this work. All authors developed the final manuscript.

Availability of data and materials Requests for materials should be addressed to Zaky A. Zaky.

Declarations

Ethics approval This article does not contain any studies involving animals or human participants performed by any of the authors.

References

Abd El-Ghany, S.E., Noum, W.M., Matar, Z., Zaky, Z.A., Aly, A.H.: Optimized bio-photonic sensor using 1D-photonic crystals as a blood hemoglobin sensor. Phys. Scr. **96**, 035501 (2020). https://doi.org/10.1088/1402-4896/abd49c

Abueidda, D.W., Elhebeary, M., Shiang, C.-S.A., Pang, S., Al-Rub, R.K.A., Jasiuk, I.M.: Mechanical properties of 3D printed polymeric Gyroid cellular structures: experimental and finite element study. Mater. Des. **165**, 107597 (2019). https://doi.org/10.1016/j.matdes.2019.107597

Ahmed, A.M., Shaban, M., Aly, A.H.: Electro-optical tenability properties of defective one-dimensional photonic crystal. Optik **145**, 121–129 (2017)

Aly, A.H., Sayed, H.: Enhancement of the solar cell based on nanophotonic crystals. J. Nanophotonics **11**, 046020 (2017)

Aly, A.H., Zaky, Z.A.: Ultra-sensitive photonic crystal cancer cells sensor with a high-quality factor. Cryogenics **104**, 102991 (2019). https://doi.org/10.1016/j.cryogenics.2019.102991

Aly, A.H., Zaky, Z.A., Shalaby, A.S., Ahmed, A.M., Vigneswaran, D.: Theoretical study of hybrid multifunctional one-dimensional photonic crystal as a flexible blood sugar sensor. Phys. Scr. **95**, 035510 (2020). https://doi.org/10.1088/1402-4896/ab53f5

Aly, A.H., Mohamed, D., Zaky, Z.A., Matar, Z.S., Abd El-Gawaad, N.S., Shalaby, A.S., et al.: Novel biosensor detection of tuberculosis based on photonic band gap materials. Mater. Res. Ibero Am. J. Mater. **24**, e20200483 (2021). https://doi.org/10.1590/1980-5373-MR-2020-0483

Aly, A.H., Awasthi, S., Mohamed, A., Matar, Z., Mohaseb, M., Al-Dossari, M., et al.: Detection of reproductive hormones in females by using 1D photonic crystal-based simple reconfigurable biosensing design. Crystals **11**, 1533 (2021b). https://doi.org/10.3390/cryst11121533

Auguié, B., Fuertes, M.C., Angelomé, P.C., Abdala, N.L., Soler-Illia, G.J., Fainstein, A.: Tamm plasmon resonance in mesoporous multilayers: toward a sensing application. ACS Photon. **1**, 775–780 (2014). https://doi.org/10.1021/ph5001549

Ayyanar, N., Raja, G.T., Sharma, M., Kumar, D.S.: Photonic crystal fiber-based refractive index sensor for early detection of cancer. IEEE Sens. J. **18**, 7093–7099 (2018). https://doi.org/10.1109/JSEN.2018.2854375

Bikbaev, R.G., Vetrov, S.Y., Timofeev, I.V.: Optical Tamm states at the interface between a photonic crystal and a gyroid layer. J. Opt. Soc. Am. B **34**, 2198–2202 (2017). https://doi.org/10.1364/JOSAB.34.002198

Bludov, Y.V., Ferreira, A., Peres, N.M., Vasilevskiy, M.I.: A primer on surface plasmon-polaritons in graphene. Int. J. Mod. Phys. B **27**, 1341001 (2013). https://doi.org/10.1142/S0217979213410014

Born, M., Wolf, E.: Principles of Optics: Electromagnetic Theory of Propagation, Interference and Diffraction of Light. Elsevier, Amsterdam (2013)

Cebo, T., Aria, A.I., Dolan, J.A., Weatherup, R.S., Nakanishi, K., Kidambi, P.R., et al.: Chemical vapour deposition of freestanding sub-60 nm graphene gyroids. Appl. Phys. Lett. **111**, 253103 (2017)

Farah, P., Demetriadou, A., Salvatore, S., Vignolini, S., Stefik, M., Wiesner, U., et al.: Ultrafast nonlinear response of gold gyroid three-dimensional metamaterials. Phys. Rev. Appl. **2**, 044002 (2014). https://doi.org/10.1103/PhysRevApplied.2.044002

Feng, Z., Li, Y., Xin, C., Tang, D., Xiong, W., Zhang, H.: Fabrication of graphene-reinforced nanocomposites with improved fracture toughness in net shape for complex 3D structures via digital light processing. C J Carbon Res **5**, 25 (2019). https://doi.org/10.3390/c5020025

Gellermann, W., Kohmoto, M., Sutherland, B., Taylor, P.: Localization of light waves in Fibonacci dielectric multilayers. Phys. Rev. Lett. **72**, 633–636 (1994)

He, Z., Cui, W., Ren, X., Li, C., Li, Z., Xue, W., et al.: Ultra-high sensitivity sensing based on tunable plasmon-induced transparency in graphene metamaterials in terahertz. Opt. Mater. **108**, 110221 (2020). https://doi.org/10.1016/j.optmat.2020.110221

Hensleigh, R.M., Cui, H., Oakdale, J.S., Jianchao, C.Y., Campbell, P.G., Duoss, E.B., et al.: Additive manufacturing of complex micro-architected graphene aerogels. Mater. Horiz. **5**, 1035–1041 (2018). https://doi.org/10.1039/C8MH00668G

Huang, X., Cao, M., Wang, D., Li, X., Fan, J., Li, X.: Broadband polarization-insensitive and oblique-incidence terahertz metamaterial absorber with multi-layered graphene. Opt. Mater. Express **12**, 811–822 (2022)

Jung, G.S., Yeo, J., Tian, Z., Qin, Z., Buehler, M.J.: Unusually low and density-insensitive thermal conductivity of three-dimensional gyroid graphene. Nanoscale **9**, 13477–13484 (2017). https://doi.org/10.1039/C7NR04455K

Katsidis, C.C., Siapkas, D.I.: General transfer-matrix method for optical multilayer systems with coherent, partially coherent, and incoherent interference. Appl. Opt. **41**, 3978–3987 (2002)

Keshavarz, M.M., Alighanbari, A.: Terahertz refractive index sensor based on Tamm plasmon-polaritons with graphene. Appl. Opt. **58**, 3604–3612 (2019). https://doi.org/10.1364/AO.58.003604

Li, Z., Peng, X., Hu, G., Zhang, D., Xu, Z., Peng, Y., et al.: Towards real-time self-powered sensing with ample redundant charges by a piezostack-based frequency-converted generator from human motions. Energy Convers. Manage. **258**, 115466 (2022)

Liu, K., Chen, Y.-M., Policastro, G.M., Becker, M.L., Zhu, Y.: Three-dimensional bicontinuous graphene monolith from polymer templates. ACS Nano **9**, 6041–6049 (2015). https://doi.org/10.1021/acsnano.5b01006

Lu, C., Zhou, H., Li, L., Yang, A., Xu, C., Ou, Z., et al.: Split-core magnetoelectric current sensor and wireless current measurement application. Measurement **188**, 110527 (2022). https://doi.org/10.1016/j.measurement.2021.110527

Luo, G., Zhang, Q., Li, M., Chen, K., Zhou, W., Luo, Y., et al.: A flexible electrostatic nanogenerator and self-powered capacitive sensor based on electrospun polystyrene mats and graphene oxide films. Nanotechnology **32**, 405402 (2021)

Lv, Z., Chen, D., Feng, H., Wei, W., Lv, H.: Artificial intelligence in underwater digital twins sensor networks. ACM Trans. Sens. Netw. (TOSN) **18**, 1–27 (2022). https://doi.org/10.1145/3519301

Ma, S., Tang, Q., Feng, Q., Song, J., Han, X., Guo, F.: Mechanical behaviours and mass transport properties of bone-mimicking scaffolds consisted of gyroid structures manufactured using selective laser melting. J. Mech. Behav. Biomed. Mater. **93**, 158–169 (2019). https://doi.org/10.1016/j.jmbbm.2019.01.023

Meradi, K.A., Tayeboun, F., Guerinik, A., Zaky, Z.A., Aly, A.H.: Optical biosensor based on enhanced surface plasmon resonance: theoretical optimization. Opt. Quant. Electron. **54**, 1–11 (2022). https://doi.org/10.1007/s11082-021-03504-8

Nakanishi, K., Labonte, D., Cebo, T., Veigang-Radulescu, V.P., Fan, Y., Brennan, B., et al.: Mechanical properties of the hollow-wall graphene gyroid lattice. Acta Mater. **201**, 254–265 (2020). https://doi.org/10.1016/j.actamat.2020.09.077

Panda, A., Devi, P.P.: Photonic crystal biosensor for refractive index based cancerous cell detection. Opt. Fiber Technol. **54**, 102123 (2020). https://doi.org/10.1016/j.yofte.2019.102123

Pandey, J.: Fibonacci quasiperiodic multilayers with internal symmetry. IOSR J Appl Phys (IOSR-JAP) **9**, 59–63 (2017)

Prayakarao, S., Robbins, S., Kinsey, N., Boltasseva, A., Shalaev, V., Wiesner, U., et al.: Gyroidal titanium nitride as nonmetallic metamaterial. Opt. Mater. Express **5**, 1316–1322 (2015). https://doi.org/10.1364/OME.5.001316

Rezagholizadeh, E., Biabanifard, M., Borzooei, S.: Analytical design of tunable THz refractive index sensor for TE and TM modes using graphene disks. J. Phys. D Appl. Phys. **53**, 295107 (2020). https://doi.org/10.1088/1361-6463/ab85e6

Salem, M., Sailor, M., Harraz, F., Sakka, T., Ogata, Y.: Electrochemical stabilization of porous silicon multilayers for sensing various chemical compounds. J. Appl. Phys. **100**, 083520 (2006). https://doi.org/10.1063/1.2360389

Sheng, H., Cong, R., Yang, D., Chen, R., Wang, S., Cui, Z.: UrbanLF: A comprehensive light field dataset for semantic segmentation of urban scenes. IEEE Trans. Circuits Syst. Video Technol. (2022). https://doi.org/10.1109/TCSVT.2022.3187664

Shukla, M.K., Das, R.: Tamm-plasmon polaritons in one-dimensional photonic quasi-crystals. Opt. Lett. **43**, 362–365 (2018). https://doi.org/10.1364/OL.43.000362

Steurer, W., Sutter-Widmer, D.: Photonic and phononic quasicrystals. J. Phys. D Appl. Phys. **40**, R229–R247 (2007)

Tammam, M.T., Zaky, Z.A., Sharma, A., Matar, Z.S., Aly, A., Mohaseb, M.A.: Defected photonic crystal array using porous GaN as malaria sensor. IOP Conf. Ser. Mater. Sci. Eng. **1171**, 012005 (2021). https://doi.org/10.1088/1757-899X/1171/1/012005

Turner, M.D., Saba, M., Zhang, Q., Cumming, B.P., Schröder-Turk, G.E., Gu, M.: Miniature chiral beamsplitter based on gyroid photonic crystals. Nat. Photon. **7**, 801–805 (2013). https://doi.org/10.1038/nphoton.2013.233

Wang, Z., Zhang, J., Xu, S., Wang, L., Cao, Z., Zhan, P., et al.: 1D partially oxidized porous silicon photonic crystal reflector for mid-infrared application. J. Phys. D Appl. Phys. **40**, 4482–4484 (2007). https://doi.org/10.1088/0022-3727/40/15/016

Yablonovitch, E.: Photonic crystals: semiconductors of light. Sci. Am. **285**, 46–55 (2001). https://doi.org/10.1038/scientificamerican1201-46

Yablonovitch, E., Gmitter, T.: Photonic band structure: the face-centered-cubic case. Phys. Rev. Lett. **63**, 1950–1953 (1989). https://doi.org/10.1103/PhysRevLett.63.1950

Ye, Y., Xie, M., Tang, J., Ouyang, J.: Highly sensitive and tunable terahertz biosensor based on optical Tamm states in graphene-based Bragg reflector. Results Phys. **15**, 102779 (2019). https://doi.org/10.1016/j.rinp.2019.102779

Yeh, P.: Optical Waves in Layered Media. Wiley, New York (1988)

Zaky, Z.A., Aly, A.H.: Theoretical study of a tunable low-temperature photonic crystal sensor using dielectric-superconductor nanocomposite layers. J. Supercond. Novel Magn. **33**, 2983–2990 (2020). https://doi.org/10.1007/s10948-020-05584-1

Zaky, Z.A., Aly, A.H.: Highly sensitive salinity and temperature sensor using Tamm resonance. Plasmonics **16**, 2315–2325 (2021a). https://doi.org/10.1007/s11468-021-01487-6

Zaky, Z.A., Aly, A.H.: Gyroidal graphene/porous silicon array for exciting optical Tamm state as optical sensor. Sci. Rep. **11**, 19389 (2021b). https://doi.org/10.1038/s41598-021-98305-0

Zaky, Z.A., Aly, A.H.: Modeling of a biosensor using Tamm resonance excited by graphene. Appl. Opt. **60**, 1411–1419 (2021c). https://doi.org/10.1364/AO.412896

Zaky, Z.A., Aly, A.H.: Novel smart window using photonic crystal for energy saving. Sci. Rep. **12**, 1–9 (2022). https://doi.org/10.1038/s41598-022-14196-9

Zaky, Z.A., Ahmed, A.M., Shalaby, A.S., Aly, A.H.: Refractive index gas sensor based on the Tamm state in a one-dimensional photonic crystal: theoretical optimisation. Sci. Rep. **10**, 9736 (2020). https://doi.org/10.1038/s41598-020-66427-6

Zaky, Z.A., Aly, A.H., Moustafa, B.: Plasma cell sensor using photonic crystal cavity. Opt. Quant. Electron. **53**, 591 (2021a). https://doi.org/10.1007/s11082-021-03201-6

Zaky, Z.A., Ahmed, A.M., Aly, A.H.: Remote temperature sensor based on tamm resonance. Silicon **14**, 2765–2777 (2021b). https://doi.org/10.1007/s12633-021-01064-w

Zaky, Z.A., Sharma, A., Alamri, S., Saleh, N., Aly, A.H.: Detection of fat concentration in milk using ternary photonic crystal. Silicon **14**, 6063–6073 (2021c). https://doi.org/10.1007/s12633-021-01379-8

Zaky, Z.A., Sharma, A., Aly, A.H.: Tamm plasmon polariton as refractive index sensor excited by Gyroid metals/porous Ta_2O_5 photonic crystal. Plasmonics **17**, 681–691 (2021). https://doi.org/10.1007/s11468-021-01559-7

Zaky, Z.A., Sharma, A., Aly, A.H.: Gyroidal graphene for exciting Tamm plasmon polariton as refractive index sensor: theoretical study. Opt. Mater. **122**, 111684 (2021e). https://doi.org/10.1016/j.optmat.2021.111684

Zaky, Z.A., Sharma, A., Alamri, S., Aly, A.H.: Theoretical evaluation of the refractive index sensing capability using the coupling of Tamm-Fano resonance in one-dimensional photonic crystals. Appl. Nanosci. **11**, 2261–2270 (2021f). https://doi.org/10.1007/s13204-021-01965-7

Zaky, Z.A., Panda, A., Pukhrambam, P.D., Aly, A.H.: The impact of magnetized cold plasma and its various properties in sensing applications. Sci. Rep. **12**, 3754 (2022a). https://doi.org/10.1038/s41598-022-07461-4

Zaky, Z.A., Alamri, S., Zhaketov, V., Aly, A.H.: Refractive index sensor with magnified resonant signal. Sci. Rep. **12**, 13777 (2022b). https://doi.org/10.1038/s41598-022-17676-0

Zaky, Z.A., Hanafy, H., Panda, A., Pukhrambam, P.D., Aly, A.H.: Design and analysis of gas sensor using tailorable Fano resonance by coupling between Tamm and defected mode resonance. Plasmonics (2022). https://doi.org/10.1007/s11468-022-01699-4

Zaky, Z.A., Al-Dossari, M., Matar, Z., Aly, A.H.: Effect of geometrical and physical properties of cantor structure for gas sensing applications. Synth. Met. **291**, 117167 (2022d). https://doi.org/10.1016/j.synthmet.2022.117167

Zaky, Z.A., Singh, M.R., Aly, A.H.: Tamm resonance excited by different metals and graphene. Photon. Nanostruct. Fundam. Appl. **49**, 100995 (2022). https://doi.org/10.1016/j.photonics.2022.100995

Zaky, Z.A., Amer, H.A., Suthar, B., Aly, A.H.: Gas sensing applications using magnetized cold plasma multilayers. Opt. Quant. Electron. **54**, 217 (2022f). https://doi.org/10.1007/s11082-022-03594-y